Hindawi
International Journal of Photoenergy
Volume 2023, Article ID 4588407, 13 pages
https://doi.org/10.1155/2023/4588407

Research Article

Influence of Duct Configurations on the Performance of Solar-Assisted Heat Pump Dryer for Drying Tobacco Leaves

Salum Abdulkarim Suleiman, Alexander Pogrebnoi, and Thomas T. Kivevele

School of Materials, Energy, Water and Environmental Sciences (MEWES), The Nelson Mandela African Institution of Science and Technology, P.O. Box 447, Arusha, Tanzania

Correspondence should be addressed to Thomas T. Kivevele; thomas.kivevele@nm-aist.ac.tz

Received 2 November 2022; Revised 20 April 2023; Accepted 5 May 2023; Published 16 May 2023

Academic Editor: Francesco Riganti-Fulginei

In the present study, a solar-assisted heat pump dryer (SAHPD) has been designed, fabricated, and tested its performance on drying tobacco leaves. The hot air generated from the solar collector and condenser unit of the heat pump was used as a source of heat in the drying chamber. In this study, we investigated the influence of three duct configurations (open, partially closed, and completely closed) on the thermal performance of SAHPD to establish the best configuration for drying tobacco leaves. The average drying temperature was found to be 66, 64, and 60°C; the coefficient of performance of the heat pump was 3.4, 3.2, and 3.0; the heat energy contribution from the solar collector was 6.6%, 5.0%, and 5.1% while for the condenser was 93.4%, 95.0%, and 94.9%, and electrical energy consumption was 2.3, 2.8, and 2.6 kWh, for the open, partially closed, and completely closed duct system, respectively. Based on these results, the open system demonstrated the best performance. According to the study's findings, SAHPD has been shown to be an energy-efficient method of drying tobacco leaves and is environmentally friendly as opposed to the conventional use of wood fuel, which results in environmental pollution, desertification, and deforestation.

1. Introduction

For many years, drying of biomaterial products has been used for preservation; most of the harvested products have high moisture content which is difficult for storage and maintenance for later uses [1, 2]. Therefore, drying is a crucial process in many food industries and agricultural-based economy countries to maintain quality without deteriorating biomaterial products, sum up the original taste, and uphold the nutrition values [3]. The main objective of drying is not only to remove moisture content from the product where bacteria and yeast can grow and spoil the product but also to preserve the initial properties of the products [4, 5]. The operating process of the dryer is to transfer heat from the source to the product and then to the environment. The structure of biomaterials in the drying process is changed by heating and causing moisture in the work to vaporize and change the layout. In various investigations, it has been demonstrated that the drying process has high energy consumption and in agriculture is 60%, while in wood it is around 70% [6]. For example, an average of 14 kg of wood fuel is consumed to obtain 1 kg of cured tobacco leading to a deforestation rate of 13,000 hectares per annum in Tanzania [7]. In efforts to combat this threat, the Tobacco Research Institute of Tanzania (TORITA) has managed to come up with rocket barns that use less wood 7 cubic meters to cure leaf tobacco compared to local barns that use 19 cubic meters of wood. This is a remarkable achievement in the tobacco sector as the calorific value of wood is still higher for curing tobacco compared to other identified organic briquettes that have already been tried. However, the tested barns are still inefficient, use wood fuel, and cause emissions. TORITA is therefore exploring an alternative curing source apart from wood, primarily renewable.

Besides, more efforts are taken on using renewable energy and other high-efficiency drying technologies. Many researchers suggest the use of heat pump dryers because of their high efficiency and energy-saving potential and less

negative impact on the environment due to greenhouse gases produced by the burning of fossil fuels and wood which leads to global warming [8]. However, solar dryers fail to operate when there is no active sunlight in case heat storage systems are not integrated into them. Sometimes even if heat storage systems are integrated, there are challenges related to the selection, cost, availability, and efficiency of storage materials. Heat pump dryers have been used in many countries to dry biomaterials that are sensitive to heat, and the process is controllable [5, 6]. The quality, color, and smell of the product dried by the heat pump are better than the product dried with other drying technologies such as open sun drying [9]. In order to increase the performance of the heat pump dryer and lower operating costs, solar collectors are integrated into the heat pump system to form a solar-assisted heat pump dryer (SAHPD) [5, 6].

The SAHPD application provides high energy efficiency with controllable temperature, airflow, air humidity, and enormous energy-saving potential. The application of heat pump drying technology in tobacco manufacturing has been reported elsewhere with an energy-saving potential from 20% to 50% [10, 11]. The SAHPD can exhibit a coefficient of performance (COP_{hp}) as high as four meaning that 1 kW of electric energy is needed to have a release of 4 kW of heat at the condenser for drying applications. A high COP value represents high efficiency and also equates to lower operating costs. This technology is uncommon in most African/developing countries; however, developed countries have been using it at an advanced stage based on their specific climatic conditions which cannot directly be applied to different regions. SAHPDs are affected by the change in ambient conditions; proper configuration of the duct is therefore the key in improving the performance of the dryer [6]. To the best of the authors' knowledge, the influence of duct configurations on the performance of SAHPD is not well documented. The objective of the present study is therefore to investigate the influence of duct configurations (open, partially closed, and completely closed air ducts) on the thermal performance of SAHPD to establish the best configuration for drying tobacco leaves in tropical climates. Three configurations of the SAHPD air duct were evaluated, and the best configuration was chosen on the base of drying temperature, COP_{hp}, and electrical energy consumption.

2. Material and Methods

2.1. Materials and Equipment. The SAHPD is the system where the solar collector and heat pump which consist of four main components (condenser (Cond), evaporator (Evap), compressor (Comp), and expansion valve (Exp. valve)) were integrated together as a source of heat in a drying process of biomaterial products. Other components like air blowing fans, drying chamber, and duct as air flowing path were used to support the workflow of the SAHPD as shown in Figures 1 and 2.

2.1.1. Solar Collector. The solar collector was designed as a passive gain system which was made of an absorbing black painted plate and transparent glass plate of 946 mm × 946 mm × 6 mm size and was integrated with the drying chamber as depicted in Figure 3. The frame of the solar collector was made of a mild steel sheet of 1.5 mm thickness and insulated by fiberglass materials; the inside of the surface of the chamber is painted black. The solar collector was inclined at 13 degrees facing north and placed on the top of the drying chamber to heat the biomaterial in the drying chamber. At the top of the glass, a cover of movable plywood was placed and used to isolate the solar irradiance entering the drying chamber when necessary.

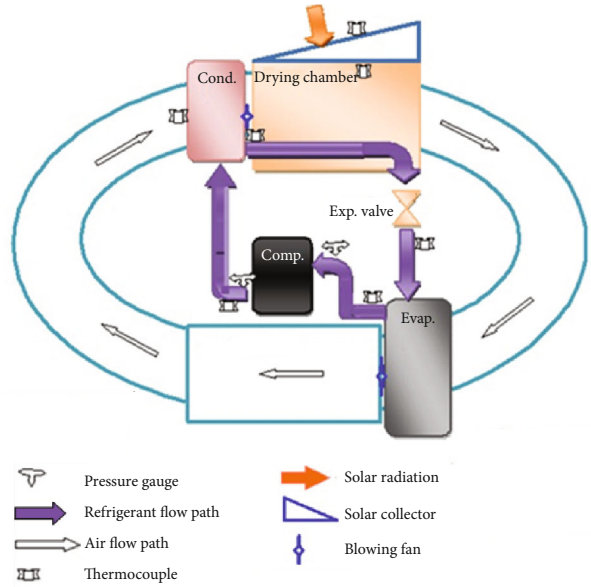

Figure 1: Schematic diagram of fully closed SAHPD.

2.1.2. Heat Pump. The heat pump is composed of a Danfoss reciprocating compressor, 4 horsepower condenser, evaporator with two built-in fans of 186 W and 0.88 A (Figure 4), and an expansion valve (3/8 × 1/2 inches) made from Denmark which is used as the pressure reducing device; the refrigerant expands and its temperature reduces. All components are connected with 3/8 and 5/8 inch copper tubes to form a single unit. The heat pump operates under refrigerant R134a (1,1,1,2-tetrafluoromethane). The refrigerant is pumped directly from the liquid receiver by the compressor in the high-pressure side; the pressurized gas passes through the condenser/heat exchanger where air entering the dryer is heated up through heat exchange between cold air passing through the surfaces of the hot copper pipes carrying hot refrigerant. The air is circulated in the system using built-in fans at the condenser and evaporator. When the latent heat of condensation of the refrigerant at the condenser is evolved, the pressured gas is condensed and accumulated at the vertical liquid receiver. The refrigerant then passes through the expansion valve which is used as the system's refrigerant control to the evaporator, creating a pressure drop and accumulating in the refrigerant receiver and then back to the low-pressure side of the compressor to complete the circulation.

For the construction of the SAHPD, the following materials available in the local market were used: tempered steel sheet and clear glass, angle irons of 25 × 25 × 3 and

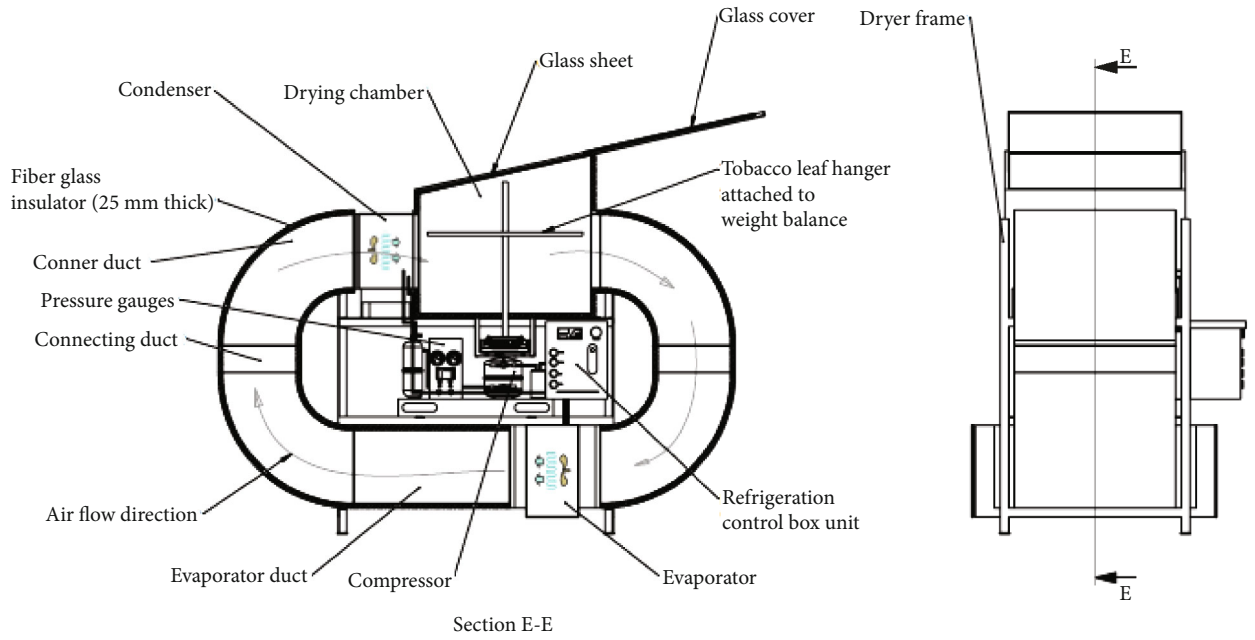

Figure 2: Section diagram of a complete solar-assisted heat pump drying system.

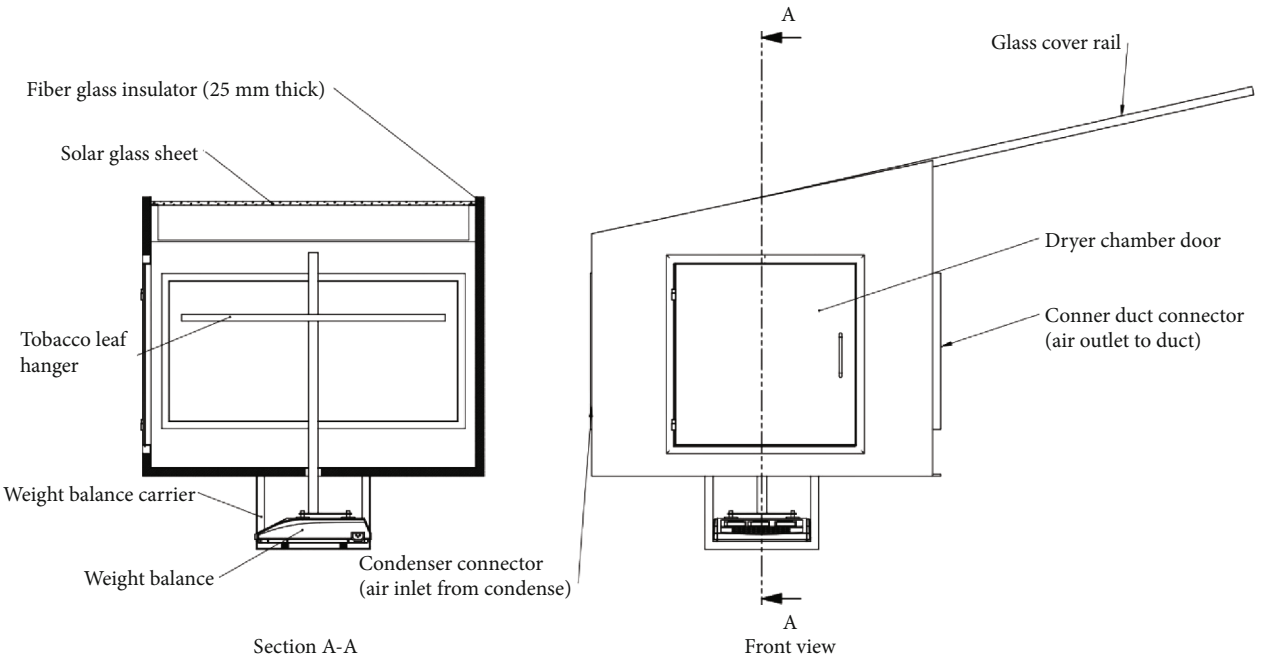

Figure 3: Section diagram of drying chamber with a solar collector.

$50 \times 50 \times 6$ mm dimensions, and aluminum rod of 40 mm diameter. The compressor and its accessories like the liquid receiver, oil receiver, and refrigerant receiver are shown in Figure 4(a). The heat pump system consists of a condensing unit, evaporator, expansion valve, and a compressor unit integrated with oil and liquid/refrigerant receivers as depicted in Figure 4, and more details are summarized in Table 1.

2.1.3. Duct. The duct system was made of a mild steel sheet of 1.5 mm thickness and reinforced by angle iron of $25 \times 25 \times 3$ mm as seen in the section diagram (Figure 5). The specification and functions of the equipment accessories are summarized in Table 1.

2.1.4. Drying Chamber. The drying chamber was a batch type made of mild steel of 1.5 mm and reinforced by angle

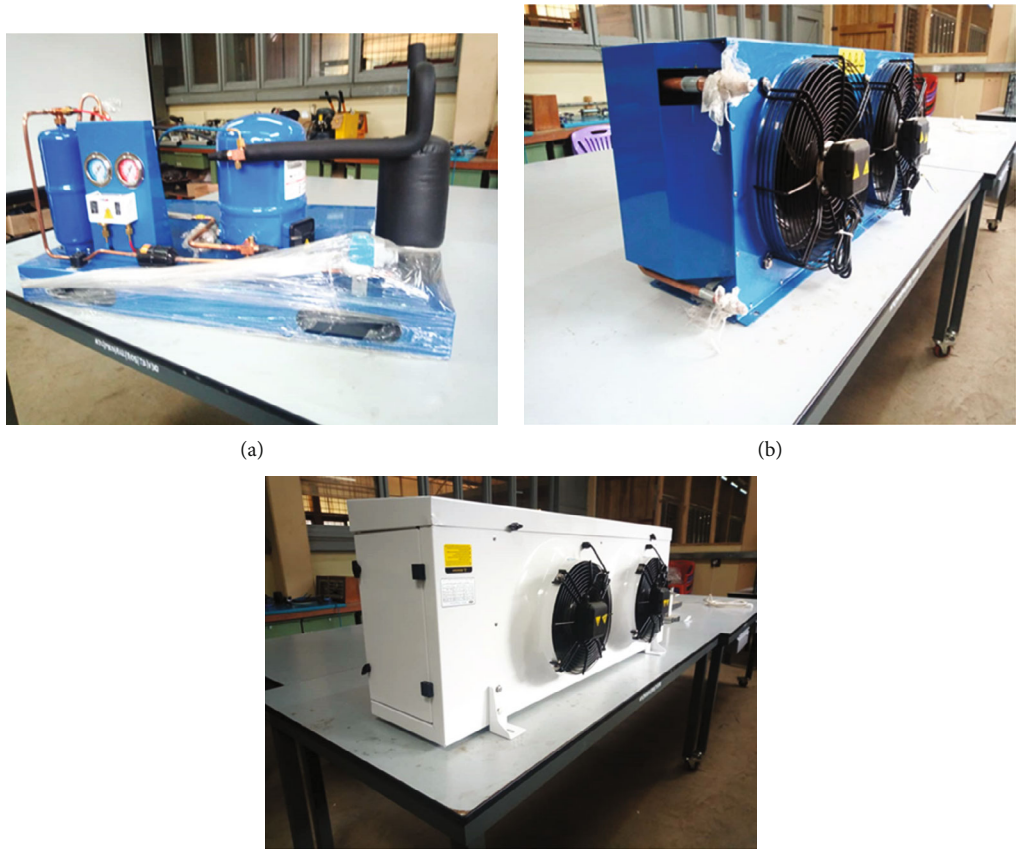

(a) (b)

(c)

Figure 4: (a) Compressor unit, (b) condenser unit, and (c) evaporator unit.

iron of $25 \times 25 \times 3$ mm for connection which was mounted by M8 and M10 bolts. The chamber was mounted on a frame made of angle iron of $50 \times 50 \times 6$ mm; at the top, it was mounted with clear glass, and one side was connected directly to the insulated duct, and the other side of it was connected to the condenser as seen in section diagram (Figure 3). The duct is connected to the evaporator, condenser, and drying chamber as depicted in Figures 1 and 4. Inside the chamber, the aluminum rod of a 40 mm radius was used as a supporter for racks on which tobacco leaves were placed (Figures 3 and 6).

Figure 3 shows the complete drying chamber integrated with a direct gain solar collector/solar glass on the top. Plywood was made to slide up and down through the glass cover rail for isolating the solar collector when only the heat pump dryer was tested. A hanger inside the drying chamber was made using the aluminum rod and flat bar sheets for hanging tobacco leaves during drying. Weight scale was placed at the bottom of the drying chamber and attached to the hanger using aluminum rod for continuously measuring the weight loss of the drying products.

2.1.5. Equipment Specifications and Functions. The equipment and accessories used for measuring temperature, pressure, relative humidity, solar radiation, and other accessories used in the SAHPD are summarized in Table 1.

2.2. Experimental Procedure

2.2.1. Three Configurations of SAHPD. The SAHPD was designed in three duct configurations, fully closed, partially closed, and fully open, as seen in Figures 1, 7(a), and 7(b), respectively. In the fully closed configuration, the air duct connects the evaporator directly with the condenser; there is no interaction between drying air and the environment, and the drying air circulates within the system without interruption as seen in the section diagram of a complete SAHPD system (Figure 2). In the partially closed configuration, there are gaps in the duct; the external air and drying air are mixed and used as inlet drying air as shown in Figure 7(a). The fully open system draws air from the fan through the evaporator and discharges air to the other end of the evaporator. It also draws the surrounding air through the condenser where it is heated and passes through the drying chamber; the moist air is discharged into the environment as shown in Figure 7(b). In this study, several parameters like temperatures (output and input temperatures of the collector ($T_{\text{o,coll}}$, $T_{\text{in,coll}}$), output and input temperatures of the condenser ($T_{\text{o,cond}}$, $T_{\text{in,cond}}$), and ambient temperature (T_{ambient})), pressures, humidity, electrical energy, solar energy, air speed, and the weight of tobacco were measured during the experiments, and these parameters were used to determine the coefficient of performance, energy consumption, and moisture content. The solar meter was used to measure solar irradiance with the solar sensor placed on a

Table 1: Equipment accessories.

S/N	Equipment	Specification	Function
1	Thermocouples	Model: T-type Max measuring temperature: 120°C and above	To measure temperatures (ambient, drying , inlet and outlet of evaporator, collector, and inlet and outlet of condenser)
2	AC Digital Display Power Monitor Meter	Voltage: 80~260 VAC rated current Power: 100 A, 22 kW Operating frequencies: 45–65 Hz	To measure the voltage, rated power, and frequency
3	FST200 Digital RS4850 10 V 0–5 V, Wind Speed Sensor Anemometer Data Logger	Model: FST200-201+211 Operating wind speed range: 0.5~50 m/s	To measure the air speed inside the drying chamber
4	21CFR Part11 Compliant USB Temperature and Humidity Data Logger Recorder with Free Software	Model: EL-21CFR-2-LCD Operating temperature range: from −35 to +80°C Relative humidity range: 0–100%	Measuring temperature and relative humidity inside the drying chamber
5	Pressure gauge	Model: CLASSES I.6 made by the XMK Company	Used to measure the pressure in the high-pressure side and low-pressure side
6	Weight balance	MX1925	Measuring the weight of tobacco leaves in the drying chamber
7	Danfoss reciprocating compressor	4 HP (MTZ36GJ5EVE, LR70 A thermal protect, low-pressure side is 22.6 bar, and high-pressure side is 29.4 bar)	Used for circulating refrigerant in the heat pump system
8	Expansion valve	R134a Danfoss (TEN2 R134a, 068Z3348, -40/+10°C/-40/+50°F)	Used as refrigerant control in a system
9	Condenser	4 HP with 102 mm × 450 mm × 300 mm dimension with two adjustable fans of 175 W, 0.75 A, and 1335 rpm	Used to condense the refrigerant vapor to liquid and for heating air entering the drying chamber
10	Evaporator	4 HP with the size of 1020 mm × 510 mm × 400 mm	Used as a heat absorption part in the system when the refrigerant passed through at low temperature and pressure
11	Refrigerant R134a	13.6 kg	Used as the refrigerant in the heat pump system
12	Solar power meter	SM206	Used to measure solar irradiance
13	Fans	175 W, 0.75 A, and 1335 rpm and 186 W and 0.88 A	Used to circulate air in the system

tilted position on the top of the solar collector surface, and the readings were recorded every 30 min; the thermocouple and multimeter were used for electrical measurements. Utilizing a weighing scale, the refrigerant R134a of 5.9 kg mass was loaded into the heat pump system; a pressure gauge was used to measure and fix pressure at the high- and low-pressure sides, 49 and 19 bar, respectively. Tobacco leaves of the same weight (15 kg) were dried in the SAHPD for each configuration. In order to maximize the thermal performance of the SAHPD, the condenser fan was run at 950 rpm from a maximum speed of 1330 rpm, and the evaporator fan was run at a minimum speed below the rated speed of 1335 rpm to reduce the cold air flowing speed because it was affecting the drying process in partially and fully closed systems. In every 30 min, the weight of the tobacco was recorded. In each experiment, sixteen measurements were taken per day. Overall, it took five weeks to complete the measurements for the aforementioned configurations, including testing, installing, and removing some components.

The drying process in the developed SAHPD employed all modes of heat transfer such as radiation, convection, and conduction. The solar collector received direct heat of short wave radiation from the sun; the collector generates the long wave radiation which combines with heated air generated from the condenser in the drying chamber [12]. Convective hot air drying involves blowing hot air over the moist products in the drying chamber. Conduction, convection, and phase change are responsible for the heat transmission from the product's surface to its inside. Mass transfer takes place through evaporation from the surface of the products to the environment as a result of the constant supply of heat energy. In addition, due to concentration gradients, internal mass transfer happens via diffusion capillary flow and viscous flow within the products [12].

(1) Evaluation of the SAHPD Performance. The SAHPD performance was evaluated through analysis of the following parameters: energy consumption, solar thermal efficiency, vapor compression in the heat pump, and efficiency of the drying chamber. All temperatures that were recorded were used in different calculations.

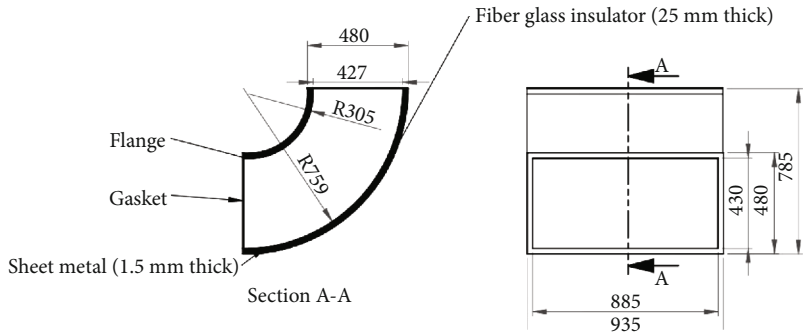

Figure 5: Section diagram of the elliptic duct.

Figure 6: Drying tobacco leaves inside the drying chamber.

2.2.2. Solar Thermal Efficiency. The solar thermal efficiency (η_{coll}), defined as the ratio of usable heat collected by the solar collector to the solar radiation received on the collector surface for a certain period, was calculated as follows [13]:

$$\eta_{\text{coll}} = \frac{\dot{m}_{\text{air}} C_{\text{pair}} (T_{\text{o,coll}} - T_{\text{in,coll}})}{I_T A_c} \times 100, \tag{1}$$

where $\dot{m}_{\text{air}}$ is the air mass flow rate, C_{pair} is the specific heat capacity of air, $T_{\text{o,coll}}$ and $T_{\text{in,coll}}$ are the outlet and inlet air temperatures of solar collector, I_T is the solar radiation incident on the collector, and A_c is the area of solar collector.

2.2.3. Performance of the Vapor Compression Heat Pump. The performance of the vapor compression heat pump cycle was determined in terms of coefficient of performance (COP_{hp}). The COP_{hp} is the ratio of the heat rejected from the condenser to the compressor work input. The COP_{hp} of the heat pump cycle was calculated through the following equation [14]:

$$\text{COP}_{\text{hp}} = \frac{Q_{\text{ucond}}}{W_{\text{comp}}}. \tag{2}$$

Simplified as

$$\text{COP}_{\text{hp}} = \frac{\dot{m}_{\text{air}} C_{\text{pair}} (T_{\text{o,cond}} - T_{\text{in,cond}})}{E_{\text{comp}}}, \tag{3}$$

where air mass flow rate is

$$\dot{m}_{\text{air}} = A_{\text{dc}} \rho_a V_{\text{air}}. \tag{4}$$

$T_{\text{o,cond}}$ and $T_{\text{in,cond}}$ are the outlet and inlet air temperatures of the condenser, and E_{comp} is the electrical energy consumed by the compressor. A_{dc}, ρ_a, and V_{air} are the area of drying chamber, air density, and air velocity, respectively. The integration of a heat pump system together with the solar collector into the dryer requires additional energy-consuming units, namely, the fans and evaporator. All the energy input to this system should be included in the calculations. Therefore, the coefficient of performance of the overall system ($\text{COP}_{\text{overall}}$) of the SAHPD was determined according to the following equation [15]:

$$\text{COP}_{\text{overall}} = \frac{Q_{\text{ucond}} + Q_{\text{ucoll}}}{E_{\text{comp}} + E_{\text{fan}}}, \tag{5}$$

where Q_{ucond} is the energy consumed by the condenser, Q_{ucoll} is the useful energy gained by the collector, and E_{fan} is the energy consumed by the fan.

Specific moisture extraction rate (SMER) which shows dehydration quantity $\dot{m}_{\text{water}}$ per unit of energy consumed was calculated by the following equation [16, 17]:

$$\text{SMER} = \frac{\dot{m}_{\text{water}}}{E_s + E_{\text{comp}} + E_{\text{fan}}}, \tag{6}$$

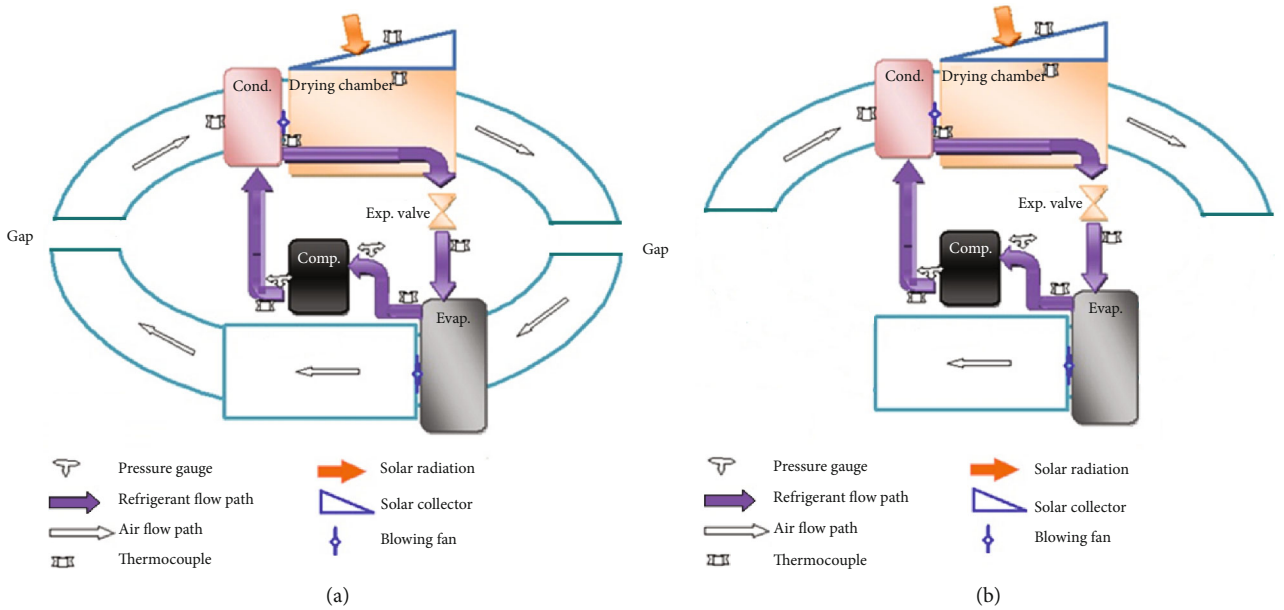

Figure 7: (a) Partially closed SAHPD. (b) Fully open SAHPD.

where E_s is the energy incident onto the plane of the solar collector.

2.2.4. Performance of Drying Chamber. The moisture content (MC) of the tobacco leaves was calculated using the following equation [16]:

$$\mathrm{MC} = \frac{m_i - m_t}{m_i} \times 100, \tag{7}$$

where m_i and m_t are the initial weights of the sample and m_t is the weight of the sample at a recorded time, respectively. The drying rate (DR) is the mass of water m evaporated from the wet tobacco leaves per unit time. It was defined using the following equation [18]:

$$\mathrm{DR} = \frac{m_{t+dt} - m_t}{dt}. \tag{8}$$

The mass of the water evaporated from wet tobacco leaves can be calculated according to [19] as

$$m = \frac{M_{\mathrm{wet}T}\left(\mathrm{MC}_i - \mathrm{MC}_f\right)}{\left(100 - \mathrm{MC}_f\right)}, \tag{9}$$

where $M_{\mathrm{wet}T}$ is the initial mass of wet tobacco leaves, MC_i is the initial, and MC_f is the final moisture content.

The thermal efficiency of a dryer is the ratio of the energy used for moisture evaporation to the energy input to the drying system. It was calculated according to [18] as follows:

$$\eta_{\mathrm{dryer}} = \frac{\dot{m}_{\mathrm{water}} H_{\mathrm{lv}}}{E_s + E_{\mathrm{comp}} + E_{\mathrm{fans}}}, \tag{10}$$

where H_{lv} is the latent heat of the vaporization of water.

The energy efficiency is the ratio of the energy consumed of the product from the drying product to the total energy input in the system and given by [15]

$$\eta_{\mathrm{energy}} = \frac{m_w H_{\mathrm{lv}}}{t_d\left(W_{\mathrm{comp+}} + W_{\mathrm{fan}}\right)}, \tag{11}$$

where m_w is the mass of water removed from the product and t_d is the drying time.

The percentage of heat energy contribution by the solar collector $\mathrm{HEC}_{\mathrm{coll}}$ and condenser $\mathrm{HEC}_{\mathrm{cond}}$ was calculated using the following equations [20]:

$$\mathrm{HEC}_{\mathrm{coll}} = \frac{Q_{\mathrm{ucoll}}}{Q_{\mathrm{ucoll}} + Q_{\mathrm{ucond}}} \times 100, \tag{12}$$

$$\mathrm{HEC}_{\mathrm{cond}} = \frac{Q_{\mathrm{ucond}}}{Q_{\mathrm{ucoll}} + Q_{\mathrm{ucond}}} \times 100, \tag{13}$$

where Q_{ucoll} is the useful heat gained by the solar collector and Q_{ucond} is the useful heat or heat energy released by the refrigerant in the condenser.

2.3. Uncertainty of Investigation Result. Uncertainty analysis is the essential analysis in any experimental work to support the obtained results, according to [15]. Let Y represent the result and $z_1, z_2, z_3, \cdots, z_n$ be the independent variables of the function. Thus,

$$Y = Y\left(z_1^{u1}, z_2^{u2}, z_3^{u3}, \cdots, z_n^{un}\right). \tag{14}$$

Table 2: Equipment and its accuracy, resolution, and error percentages.

S/N	Equipment	Accuracy	Resolution	Error (%)
1	Thermocouples	±0.5°C	±0.1°C	0.1424
2	21CFR Part11 Compliant USB Temperature and Humidity Data Logger Recorder with Free Software	±0.3 RH	±0.1 RH	0.1424
3	Solar power meter	±10 W/m^2	±0.1 W/m^2	0.1424
4	FST200 Digital RS4850 10 V 0–5 V, Wind Speed Sensor Anemometer Data Logger	±0.1 m/s	±0.05 m/s	0.0712
5	Weight balance	±0.14 g	±0.1 g	0.1424
6	Pressure gauge	±0.1 psi	±0.1 psi	0.1424

Let Q_R be the uncertainty and $Q_1, Q_2, Q_3, \cdots, Q_n$ be the uncertainty variables; then, the estimated uncertainty of the investigated parameter is calculated as

$$Q_R = \left[\left(\frac{\partial Y}{\partial z_1}Q_1\right)^2 + \left(\frac{\partial Y}{\partial z_2}Q_2\right)^2 + \cdots + \left(\frac{\partial Y}{\partial z_n}Q_n\right)^2\right]^{1/2}. \quad (15)$$

The instrumental details are explained in Table 1. The estimated relative uncertainties of the COP, moisture content, drying rate, energy efficiency, SMER, and energy contribution are ±3.39, ±4.23, ±3.60, ±3.58, ±3.28, and ± 3.18%, respectively.

Regardless of how precise and accurate a measurement is, it is typically subject to some degree of uncertainty. During the measurement, uncertainty may occur in measurement techniques or in measuring apparatus according to [21]; assessment of uncertainty is the essential analysis in any experimental work to support the obtained results [15]. The total errors were calculated by using equation (14) according to [22]. Table 2 shows the summary of the instruments used and their uncertainty assessment.

$$W_{\text{th}} = \sqrt{(Y_1)^2 + (Y_2)^2 + \cdots + (Y_n)^2}, \quad (16)$$

where W_{th} is the total instrumental uncertainty and Y is the independent variable affecting measurements.

The total uncertainty for temperature measurements from the thermocouple measurements (Z) (systematic error from manufacturer) and N as reading errors (random error) is given by equation (15) according to [22].

$$W_T = \sqrt{(Z_T)^2 + (N_T)^2}. \quad (17)$$

Total uncertainty for measurement of relative humidity (RH) was determined as follows:

$$W_{\text{RH}} = \sqrt{(Z_{\text{RH}})^2 + (N_{\text{RH}})^2}. \quad (18)$$

Total uncertainty for measurement of solar radiation (SR), wind, weighing of products, and pressure of the refrigerant was determined by equations (17), (18), (19), (20), (21), and (22), respectively, according to [23].

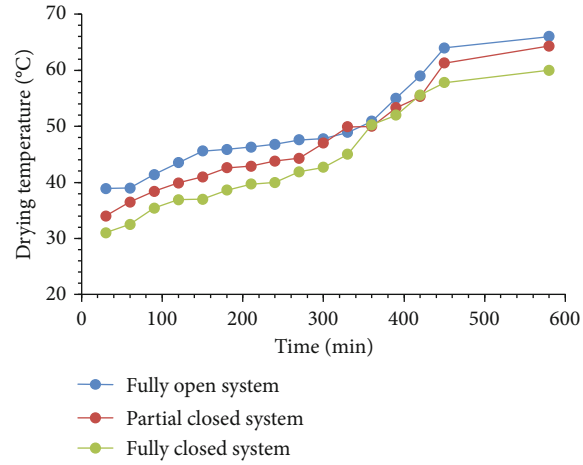

Figure 8: Drying air temperature with time.

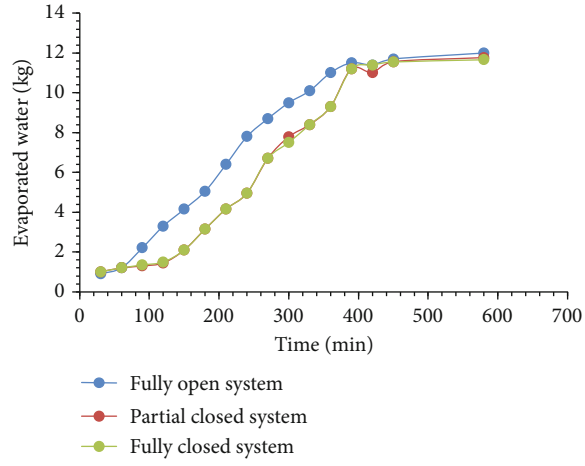

Figure 9: Mass of evaporated water vs. drying time.

$$W_{\text{SR}} = \sqrt{(Z_{\text{SR}})^2 + (N_{\text{SR}})^2}, \quad (19)$$

$$W_{\text{wind}} = \sqrt{(Z_{\text{wind}})^2 + (N_{\text{wind}})^2}, \quad (20)$$

$$W_{\text{weighing}} = \sqrt{(Z_{\text{weighing}})^2 + (N_{\text{weighing}})^2}, \quad (21)$$

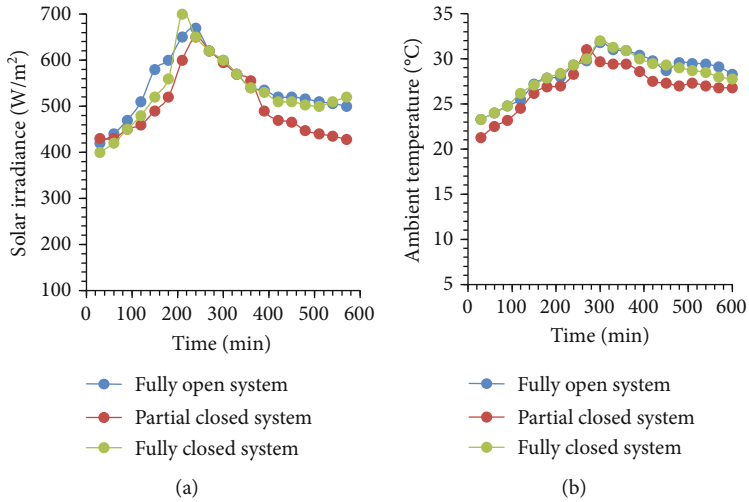

Figure 10: The variation of (a) solar irradiation and (b) ambient temperature with time.

$$W_{\text{pressure}} = \sqrt{(Z_{\text{pressure}})^2 + (N_{\text{pressure}})^2}. \quad (22)$$

The overall total uncertainty in measurement of different parameters is given by equation (23) according to [23].

$$W_{\text{total}} = \sqrt{(W_{\text{temp}})^2 + (W_{\text{RH}})^2 + (W_{\text{SR}})^2 + (W_{\text{wind}})^2 + (W_{\text{weighing}})^2 + (W_{\text{pressure}})^2}. \quad (23)$$

3. Results and Discussion

3.1. Uncertainty Analysis. The total uncertainties in the measuring instruments and reading errors are calculated according to equation (21) and found to be ±1.5% (rounded); this value is small as compared to the acceptable range of ± 10% according to Choi et al. [24].

3.2. Drying Temperature and Moisture Content. Drying air temperature measured with the thermocouple in the drying chamber versus time for three configurations is shown in Figure 8. The starting point (0 min) corresponded to 09 h00, and the experiment was finished at 10 h (600 min on the plots). In general, for the fully open system, the drying air temperature was higher due to the contribution of surroundings, whereas in partially and fully closed systems the temperature was lower because of cool air contribution from the evaporator circulating through the system. A decrease in drying temperature was observed in the first 100 minutes which was possible due to the evaporation of a rather big amount of water from wet tobacco leaves; air temperature decreased rapidly during the initial drying period for the fully open system. The drying air temperature depends on heated air from the heat pump condenser, and the heated air is delivered into the solar collector. The mass of evaporated water from 15 kg of tobacco leaf load with time is shown in Figure 9; it can be observed that for all three systems, the dry product was obtained after the same drying time, about 400 min, and approximately 12 kg of water was evaporated.

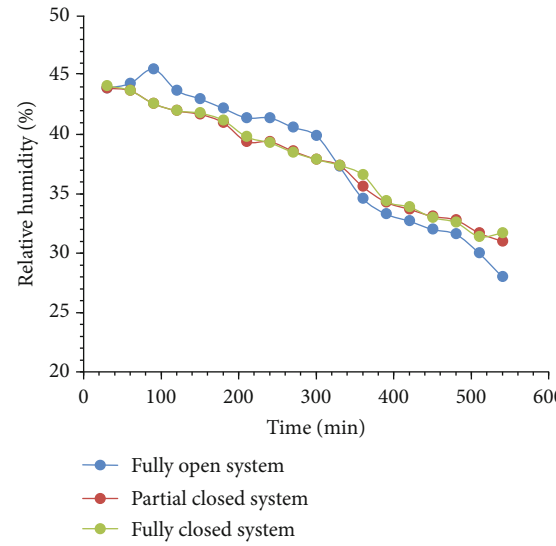

Figure 11: The relative humidity in the drying chamber vs. drying time.

Solar irradiance and ambient temperature being dependent on the climatic condition are very important parameters for drying process of tobacco leaves in the SAHPD. The solar irradiance was measured during a day when the fully open system experiment was conducted as shown in Figure 10; similar trends were observed for both parameters, and the maximum values of 670 W/m^2 and 32°C were detected for solar irradiance and ambient temperatures, respectively, close to midday.

3.3. Performance of the SAHP

3.3.1. Solar Thermal Efficiency. The solar thermal efficiency calculated using equation (1) differs throughout the day depending on the air duct configuration; the highest efficiency was recorded for the fully open air duct system (69.3%) followed by a partially and completely closed system

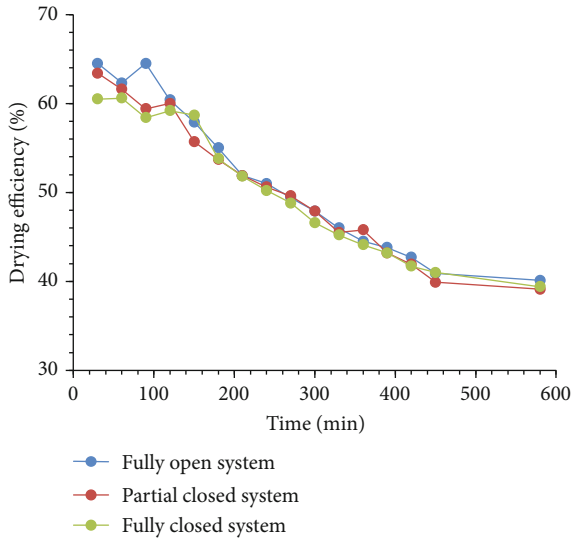

Figure 12: The thermal efficiency of a dryer vs. time.

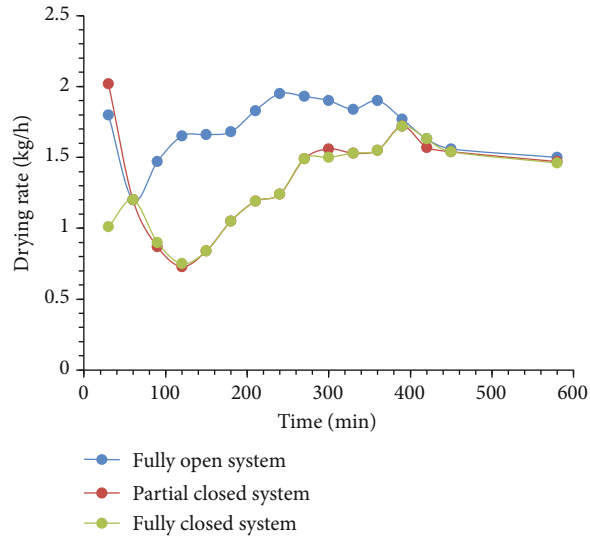

Figure 13: Drying rate vs. time.

which were 66.3% and 64.8%, respectively. The minimum thermal efficiency was 22.5%, 21.5%, and 20.8%, respectively. The thermal efficiency of solar collector varies when solar irradiance varies. The solar collector was more sensitive to solar irradiance; the solar thermal efficiency was higher for higher solar irradiance. The lower thermal efficiency recorded by a fully closed system possibly was due to the circulation of cold air from the evaporator while a fully open system was favored by high ambient temperature.

The relative humidity in the drying chamber vs. drying time is depicted in Figure 11; maximum values were 45.5, 43.9, and 43.7% for the fully open, partially closed, and fully closed systems, respectively, while minimum humidity values were equal to 28.7, 30.7, and 33.1%. Whenever the drying temperature increased, the relative humidity also decreased [25].

For the partially and fully closed systems, as compared to the fully open system, the evaporator fans significantly affected both the relative humidity and drying temperature in the drying chamber because of the circulation of cold air from the evaporator [26].

The thermal efficiency of the dryer versus drying time is shown in Figure 12. The drying efficiency was higher for moist tobacco leaves and was decreasing as the moisture reduced.

The higher drying efficiency is produced when the humidity decreases due to increase of the drying temperature [27]. Maximum drying efficiency of about 65% was observed for the fully open system.

The drying rate of the dryer for the three configurations is demonstrated in Figure 13; the average values are 1.5, 1.4, and 1.3 kg/h for fully open, partially open, and fully closed systems, respectively. The drying rate of the fully closed system starts to increase with time due to the increase of the drying temperature to a maximum and then decreases when moisture is reduced in the tobacco leaves. Initially, for some time, the drying rate of the fully open system started to decrease due to the low inlet temperature and then increases

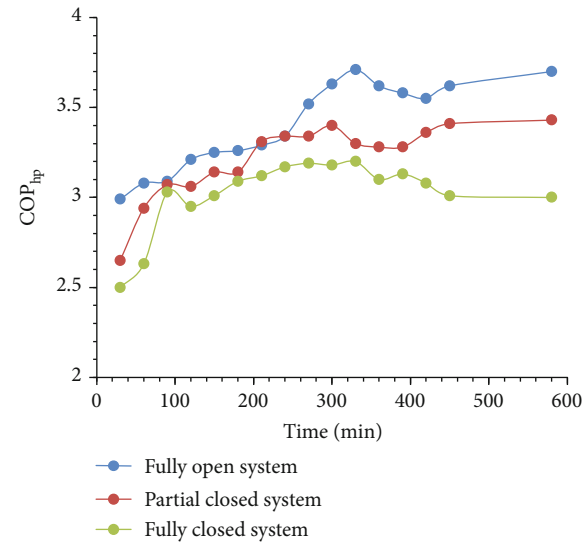

Figure 14: Variation of COP_{hp} with drying time.

with time up when the inlet temperature and dryer temperature were higher than the drying rate due to reduced moisture. It is worth noting that the highest drying rate was observed for the fully open system; this is because it exhibited higher drying temperatures and low relative humidity.

3.3.2. Performance of Vapor Compression Heat Pump. The coefficient of performance of the heat pump as calculated by equation (2) for the open, partially closed, and fully closed air duct systems is shown in Figure 14. The average values of COP_{hp} were 3.4, 3.2, and 3.0 for the open, partially closed, and fully closed air duct systems, respectively. The condenser's inlet and outlet temperatures were influenced by the surrounding conditions; the average inlet and outlet temperatures were between 28.2 and 48.4°C, 27.4 and 46.5°C, and 24.4 and 43.5°C for the fully open, partially closed, and fully closed systems, respectively. The mixing

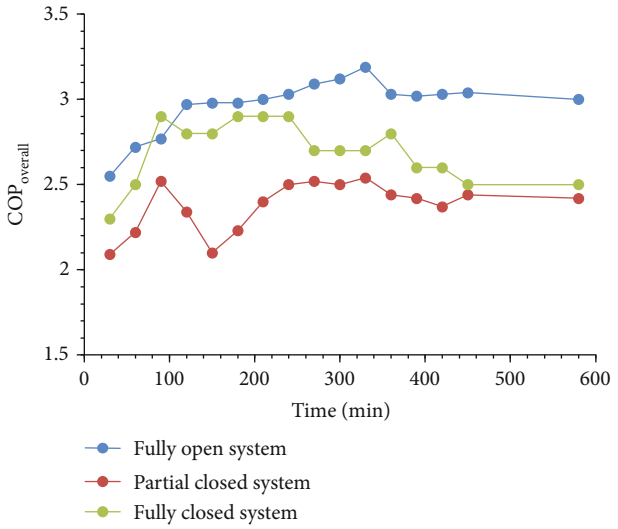

Figure 15: Variation of the overall coefficient of performance of the SAHPD with drying time.

of ambient air and cold air from the evaporator affects the condenser outlet temperature range to low values in partially and fully closed ducted system configurations, but open systems use only ambient air as the condenser inlet. The circulated air from the evaporator causes the COP_{hp} to fluctuate and affect the dryer heating capacity.

$COP_{overall}$ of the three configurations is shown in Figure 15; the minimum and maximum $COP_{overall}$ for the fully opened, partially closed, and completely closed system was 2.6 to 3.2, 2.1 to 2.5, and 2.3 to 2.9, respectively, which were calculated using equation (3). $COP_{overall}$ increased with the solar irradiance increase and reduced when solar irradiance was low [28]. $COP_{overall}$ for the open air duct system was higher than that for the other two systems. $COP_{overall}$ was lower as compared to COP_{hp} because of the inclusion of energy consumed by the evaporator and condenser fans in the calculation. Thus, the greater values of COP_{hp} and $COP_{overall}$ were observed for the fully open system.

3.4. Heat Energy Contribution. Heat energy contributions made by the solar collector and condenser as calculated using equations (9) and (10) are shown in Figures 16 and 17. The average values for the solar collector were 6.6, 5.0, and 5.1%, while for the condenser were 93.4, 95.0, and 94.9%, for open, partially closed, and fully closed systems, respectively. Solar radiation and the temperature difference between the solar collector's inlet and outlet had an impact on the heat energy contribution. The percentage of the heat energy contribution made by the condenser is increased with a decrease in the contribution of the solar collector which is in accordance with the literature [29].

The SAHPD has been made and used for drying various biomaterial in different countries with different climatic conditions, and it was observed that COP_{hp} varies from 2.28 to 4.18 as reported by Koşan et al. [30] and Akhilesh et al. [31, 32]. The SAHPD was conducted for three distinct weather conditions such as clear day, intermittent cloudy day, and overcast sky.

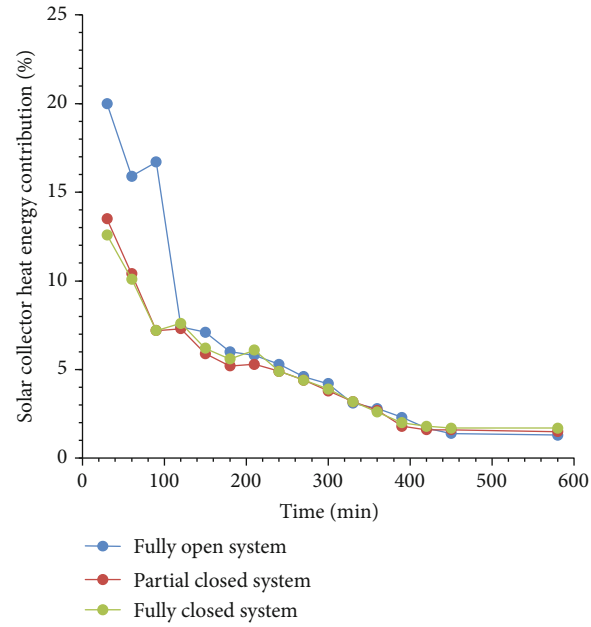

Figure 16: Variation of solar collector heat energy contribution with time.

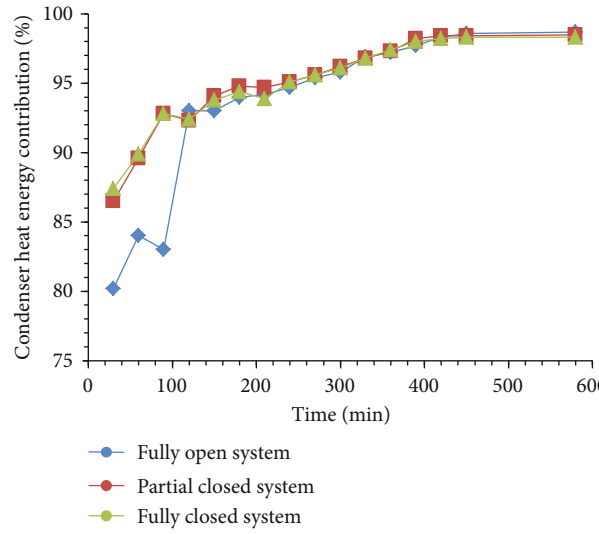

Figure 17: Variation of the heat energy contribution of the condenser with time.

4. Conclusion

The present study investigated the influence of duct configurations on the performance of the developed solar-assisted heat pump dryer (SAHPD) for drying tobacco leaves (commercial crop). Three air duct configurations (fully open, partially closed, and fully closed) were investigated, and the best confirmation was identified. In comparison to partially and fully closed systems, the fully open system was found to have a greater drying rate, 1.5 kg/h, and higher COP_{hp}, from 3.0 to 3.7. Partially and fully closed systems demonstrated lower drying performance than fully open

system because of the circulation of cold air and higher relative humidity of the drying air. While the evaporator fan impacts the temperature of air circulating in the duct in partially and totally closed systems, it increases energy consumption owing to heat recovery. The fully open systems require less resources. Therefore, for drying tobacco leaves, the fully open design outperformed the partially and completely closed configurations.

Data Availability

Data are available upon request.

Conflicts of Interest

There is no conflict of interest regarding the publication of this paper.

Acknowledgments

The authors acknowledge support from the Tanzania Commission for Science and Technology (COSTECH) under the project with reference number FA.403/489/55/4. The authors are also grateful for the support from the RSIF funded project titled "Solar-assisted heat pump dryer with energy storage for drying biomaterials (SOHEADS)" (grant reference no. RSIF/RA/001).

References

[1] A. Alishah, M. Kiamahalleh, F. Yousefi, A. Emami, and M. Kiamahalleh, "Solar-assisted heat pump drying of coriander: an experimental investigation," *International Journal of Air-Conditioning and Refrigeration*, vol. 26, no. 4, article 1850037, 2018.

[2] N. Vickers, "Animal communication: when I'm calling you, will you answer too?," *Current Biology*, vol. 27, no. 14, pp. R713–R715, 2017.

[3] K. Chua and S. Chou, "Recent advances in hybrid drying technologies," in *Emerging Technologies for Food Processing*, pp. 447–459, Elsevier, 2014.

[4] V. Sagar and P. Kumar, "Recent advances in drying and dehydration of fruits and vegetables: a review," *Journal of Food Science and Technology*, vol. 47, no. 1, pp. 15–26, 2010.

[5] X. Liu, L. Ni, S. K. Lau, and H. Li, "Performance analysis of a multi-functional heat pump system in heating mode," *Applied Thermal Engineering*, vol. 51, no. 1-2, pp. 698–710, 2013.

[6] S. Şevik, "Experimental investigation of a new design solar-heat pump dryer under the different climatic conditions and drying behavior of selected products," *Solar Energy*, vol. 105, pp. 190–205, 2014.

[7] F. Msigwa, *Impacts of tobacco production on forest resources management in Kasulu District, Tanzania*, The Open University of Tanzania, 2019.

[8] K. J. Chua, S. K. Chou, and W. M. Yang, "Advances in heat pump systems: A review," *Applied Energy*, vol. 87, no. 12, pp. 3611–3624, 2010.

[9] L. Jimu, M. Loritah, M. Lovemore, and W. Innocent, "The Miombo ecoregion up in smoke: the effect of tobacco curing," *Perspectives*, vol. 5, pp. 44–46, 2017.

[10] G. J. Newbert, "Energy efficient drying, evaporation and similar processes," *Journal of heat recovery systems*, vol. 5, no. 6, pp. 551–559, 1985.

[11] S. Ratner, G. Konstantin, R. Svetlana, and L. Inna, "Energy saving potential of industrial solar collectors in southern regions of Russia: the case of Krasnodar region," *Energies*, vol. 13, no. 4, p. 885, 2020.

[12] T. Naemsai, J. Jareanjit, and K. Thongkaew, "Experimental investigation of solar-assisted heat pump dryer with heat recovery for the drying of chili peppers," *Journal of food process engineering*, vol. 42, no. 6, article e13193, 2019.

[13] J. Kaewkiew, S. Nabnean, and S. Janjai, "Experimental investigation of the performance of a large-scale greenhouse type solar dryer for drying chilli in Thailand," *Procedia Engineering*, vol. 32, pp. 433–439, 2012.

[14] Technoheaven, *Hotel Booking System*, 2023, https://www.technoheaven.net/hotel-booking-software.aspx.

[15] A. Singh, J. Sarkar, and R. R. Sahoo, "Experimental energy, exergy, economic and exergoeconomic analyses of batch-type solar-assisted heat pump dryer," *Renewable Energy*, vol. 156, pp. 1107–1116, 2020.

[16] M. N. Hawlader, C. O. Perera, and M. Tian, "Properties of modified atmosphere heat pump dried foods," *Journal of Food Engineering*, vol. 74, no. 3, pp. 392–401, 2006.

[17] B. Q. Huy, "Experiment investigation on a solar asisted heat pump dryer for chili," *International Journal of Energy and Environmental Science*, vol. 3, no. 1, p. 37, 2018.

[18] V. Shanmugam and E. Natarajan, "Experimental study of regenerative desiccant integrated solar dryer with and without reflective mirror," *Applied Thermal Engineering*, vol. 27, no. 8-9, pp. 1543–1551, 2007.

[19] N. Srisittipokakun, K. Kirdsiri, and J. Kaewkhao, "Solar drying of Andrographis paniculata using a parabolicshaped solar tunnel dryer," *Procedia Engineering*, vol. 32, pp. 839–846, 2012.

[20] E. Kush, "Performance of heat pumps at elevated evaporating temperatures with application to solar input," *Journal of Solar Energy Engineering*, vol. 102, no. 3, pp. 203–210, 1980.

[21] A. Ahmad and O. Prakash, "Performance evaluation of a solar greenhouse dryer at different bed conditions under passive mode," *Journal of Solar Energy Engineering*, vol. 142, no. 1, 2020.

[22] F. Gulcimen, H. Karakaya, and A. Durmus, "Drying of sweet basil with solar air collectors," *Renewable energy*, vol. 93, pp. 77–86, 2016.

[23] A. R. U. Sundari and E. Veeramanipriya, "Performance evaluation, morphological properties and drying kinetics of untreated Carica papaya using solar hybrid dryer integrated with heat storage material," *Journal of Energy Storage*, vol. 55, article 105679, 2022.

[24] W. Choi, H. Kikumoto, R. Choudhary, and R. Ooka, "Bayesian inference for thermal response test parameter estimation and uncertainty assessmen," *Applied Energy*, vol. 209, pp. 306–321, 2018.

[25] H.-Y. Ju, Z. Shi-Hao, A. Mujumdar et al., "Energy efficient improvements in hot air drying by controlling relative humidity based on Weibull and Bi-Di models," *Food and Bioproducts Processing*, vol. 111, pp. 20–29, 2018.

[26] S. Krishnamoorthy, M. Mark, and H. Curtis, "Efficiency optimization of a variable-capacity/variable-blower-speed residential heat-pump system with ductwork," *Energy and Buildings*, vol. 150, pp. 294–306, 2017.

[27] A. Singh, J. Sarkar, and R. R. Sahoo, "Experimental performance analysis of novel indirect-expansion solar-infrared assisted heat pump dryer for agricultural products," *Solar Energy*, vol. 206, pp. 907–917, 2020.

[28] B. Luo, Z. Peng, J. Tao, G. Qun, and L. Jingping, "Decoupled duplex Stirling machine: conceptual design and theoretical analysis," *Energy Conversion and Management*, vol. 210, article 112704, 2020.

[29] C. Li, L. Jiangwei, Z. Siyang, C. Xingyu, J. Li, and Z. Zhiyong, "Performance analysis of an improved power generation system utilizing the cold energy of Lng and solar energy," *Applied Thermal Engineering*, vol. 159, article 113937, 2019.

[30] M. Koşan, M. Demirtaş, M. Aktaş, and E. Dişli, "Performance analyses of sustainable Pv/T assisted heat pump drying system," *Solar Energy*, vol. 199, pp. 657–672, 2020.

[31] S. Akhilesh, S. Jahar, and S. Rashmi, "Experimental energy-exergy performance and kinetics analyses of compact dual-mode heat pump drying of food chips," *Journal of Food Process Engineering*, vol. 43, no. 6, article e13404, 2020.

[32] S. Akhilesh, S. Jahar, and S. Rashmi, "Experimentation on solar-assisted heat pump dryer: thermodynamic, economic and exergoeconomic assessments," *Solar Energy*, vol. 208, pp. 150–159, 2020.